ELSEVIER

Materials Science and Engineering B101 (2003) 60–64

MATERIALS SCIENCE & ENGINEERING B

www.elsevier.com/locate/mseb

# Laser-induced treatment of silicon in air and formation of Si/$SiO_x$ photoluminescent nanostructured layers

A.V. Kabashin *, M. Meunier

*Laser Processing Laboratory, Department of Engineering Physics, Ecole Polytechnique de Montréal, Case Postale 6079, succ. Centre-ville, Montréal, Québec, Canada H3C 3A7*

**Abstract**

Two different mechanisms of laser-induced treatment of silicon in atmospheric air are compared. In one, silicon target was ablated by pulsed UV radiation, which led to a formation of microscale spikes under the irradiation spot and a deposition of material around it. The treated material contained silicon nanocrystals and exhibited weak photoluminescence (PL) signals, whose peak position was not uniform over the treated surface and varied from 2.0 to 2.3 eV in different points. In another mechanism, silicon target served to provide first electrons in order to initiate a breakdown in surrounding air by pulsed IR radiation. As a result, a highly porous nanostructured layer was formed under the contact of the target with the breakdown plasma. All points of the layer exhibited only 1.95 eV PL signals, whose intensity was stronger than in the case of the UV ablation by at least an order of magnitude. Possible mechanisms of nanostructure formation and PL origin are discussed.


*Keywords:* Air optical breakdown; Laser ablation; Nanostructured silicon; Photoluminescence

## 1. Introduction

A combination of optoelectronics applications and silicon-based microelectronics technology is an attractive basis to develop a new generation of low-cost integrated photonic devices. However, the prospects for Si-based optoelectronics are limited by the fact that bulk silicon does not emit visible light. This natural obstacle can be overcome with the recent discovery of visible emission from nanostructured Si-based materials [1]. The nanostructuring can be produced by the anodical etching [1] and a number of dry deposition techniques such as e.g., magnetron sputtering [2], laser breakdown of silane [3], pulsed laser ablation [4–7] etc. Though the anodical etching enables one to produce nanostructured silicon with the most intense photoluminescence (PL) emission, dry techniques are considered as more adequate for creating optoelectronics devices due to their better potential compatibility with silicon processing technology.

For some applications, it is preferable to avoid depositing a nanostructured film on the entire substrate, but to produce nanostructured PL area directly on an assembled silicon-based device or integrated chip. Dry techniques to fabricate these structures are the electric spark processing [8–11] and excimer laser annealing of amorphous silicon films [12,13]. As one of the alternative possibilities, we have recently introduced air optical breakdown processing [14], which is a very simple, dry, fast and vacuum-free method for local patterning of PL structures. Infrared (IR) radiation was focused on a silicon wafer in atmospheric air. The target served to produce first electrons to initiate the air optical breakdown, which then developed in ambient gas toward the focusing lens. Absorbing main radiation and getting heated to temperatures of $10^4$ K for milliseconds [15], the air optical breakdown plasma served as an efficient source to modify the properties of Si-based material and form the porous nanostructured layers, exhibiting strong PL in red. The air optical breakdown processing does not use high voltages and does not require a preliminary film deposition, as in

* Corresponding author. Tel.: +1-514-340-4711x4634; fax: +1-514-340-3218.

*E-mail address:* akabach@email.phys.polymtl.ca (A.V. Kabashin).

0921-5107/03/$ - see front matter 
doi:10.1016/S0921-5107(02)00651-7

experiments with electric spark processing [8–11] and excimer laser annealing of amorphous silicon films [13,14], respectively.

In this paper, we compare air optical breakdown processing with the case of direct material ablation in atmospheric air. For the ablation experiments, we used UV radiation, which is strongly absorbed by the target and is almost transparent for the plasma. Structural and PL properties of the layers produced by two methods are considered.

## 2. Experimental setup

For ablation experiments, we used the radiation of a pulsed KrF laser ($\lambda = 248$ nm, pulse length 15 ns FWHM, repetition rate 30 Hz), which was normally focused onto a Si target in air. Under the irradiation spot size of $2 \times 1$ mm$^2$, the radiation intensity was about $5 \times 10^8$ W cm$^{-2}$, which was sufficient to produce the laser plasma in the atmospheric pressure air. For breakdown experiments, we used the radiation of pulsed TEA $CO_2$ laser (wavelength 10.6 μm, pulse energy 1 J, pulse length 1 μs FWHM, repetition rate 3 Hz), which was focused by a Fresnel's lens onto a silicon target in air. The target was placed in different positions from $z = -20$ to $z = 20$ mm, where $z = 0$ corresponds to the focal plane. The IR radiation intensity at the focal plane was about $10^8$ W cm$^{-2}$. Standard silicon wafers (n- and p-type, resistances 0.01–10 Ω cm) with dimensions about $1 \times 1$ cm$^2$ were used as targets. Experiments were carried out in atmospheric air (1 atm., 20 °C, 40% humidity).

Scanning electron microscopy (SEM) was used to examine structural properties of the films. The surface composition of the layers was analyzed by X-ray photoemission spectroscopy (XPS) using a thermo VG scientific system. In addition, X-ray diffraction (XRD) spectroscopy was used to examine the crystallinity and the porosity of the films. The PL spectra were measured at room temperature. The samples were illuminated by the radiation of a cw $Ar^+$ laser with the wavelength 488 nm. The power was 10 mW and the power density was estimated to be 30 W cm$^{-2}$. The spectra were corrected to take into account the spectral response of the PL setup.

## 3. Results

For both cases, the radiation-target interaction was accompanied by a plasma production. However, in the case of the excimer laser the plasma was localized less than 2 mm from the target surface, whereas for the $CO_2$ one it propagated up to the distances of 0.5–2 cm from the target to the focusing lens forming a flashing line in air. Such a long visible size of plasma in the case of $CO_2$ laser is apparently related to the efficient absorption of IR radiation in the breakdown forefront through the inverse Bremstrahlund mechanism [15]. The breakdown propagated toward the focusing lens and was supported by the ionization of cold gas. In contrast, the UV radiation from the excimer laser was absorbed by the target itself and the forming plasma remained transparent to the UV during the laser pulse. Therefore, the plasma remained located near the target, while no discharge developed in the cold gas. We also observed that the plasma intensity raised with the number of laser shots. The effect was especially remarkable in the case of the $CO_2$ radiation. The intensity gain was apparently connected to an appearance of mechanical defects on the target surface, which improved the radiation absorption.

The ablation of the target by several pulses of the excimer laser led to a formation of a crater under the irradiation spot and to a deposit surrounding the crater. The bottom and walls of the crater contained microscale spikes, which were oriented along the incident beam as shown in Fig. 1(a). The height of the spikes increased

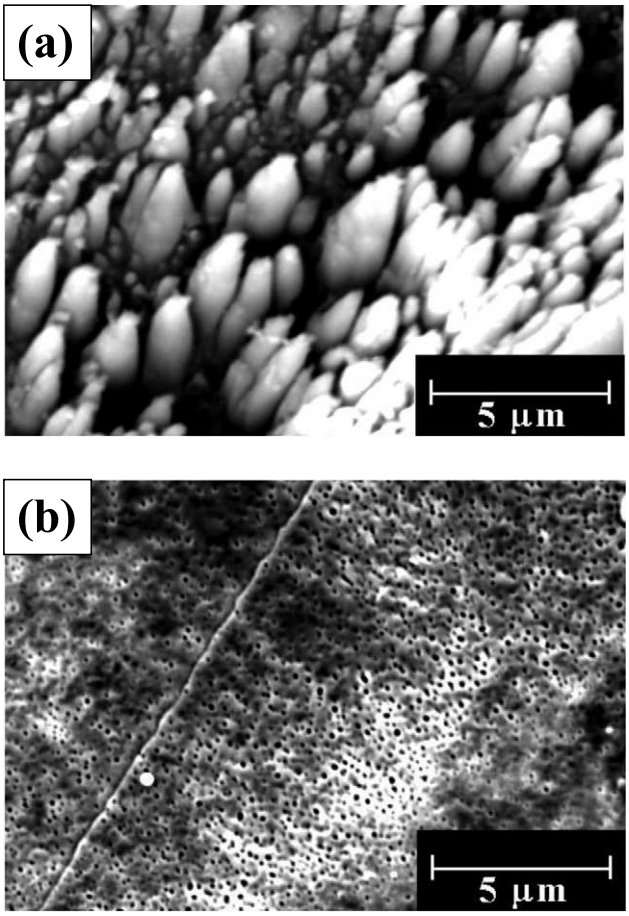


Fig. 1. SEM images of a silicon target after its irradiation by 200 pulses of the excimer (a) and $CO_2$ (b) laser near the plasma ignition threshold.

with the number of laser shots at the same irradiation spot and could reach 5–7 μm. It should be noted that similar spikes in the crater were observed in many previous papers on laser ablation [16]. The target irradiation by several pulses of $CO_2$ laser led to quite different surface modifications. In this case, the crater was not formed, while the deposition of material on the free target surface was weak or not visible by SEM at all. Furthermore, the irradiated surface did not contain any spikes. In contrast, it was a highly porous structure, containing holes with the minimal size of several dozens of nanometers, as one can see from Fig. 1(b). The pore size did not change with the number of laser shots at the same irradiation spot. In contrast to the excimer laser ablation, the treated surface contained cracks, as one can see from Fig. 1(b).

XPS spectra of samples prepared by both the laser ablation and the breakdown processing showed a single peak at 104 eV. This peak is always assigned to 2p photoelectrons of pure $SiO_2$, suggesting that the processed layers mainly consisted of silicon dioxide. Nevertheless, XRD studies showed that both treatments led to peaks associated with different crystalline silicon phases, suggesting that silicon crystals are also present in the layers. This gives the evidence that the resulting layers consisted of silicon crystals embedded in $SiO_2$ matrix. It is known that the broadness of XRD peaks is mainly determined by the smallest clusters [17]. As the instrumental noises are relatively low, this property could be used to estimate roughly the minimal size of crystals in the deposit by the Debye–Scherrer formula [17]. Taking the broadness of a typical silicon peak ($\Delta(2\theta)/2 = 0.6^\circ$) from a highly resolved XRD spectrum (Fig. 2), the estimation gives a grain size of the order of 10 nm.

PL properties of the layers fabricated by the excimer and $CO_2$ laser treatment were rather different. As shown in Fig. 3(a), the surface ablated by the excimer laser yield to PL signals with the peak position between 2.0 and 2.3 eV, though their intensity was relatively weak. However, we noticed that PL signals were not uniform over the sample and differed drastically from point to point. For example, the microstructure in the crater center generally exhibited 2.2–2.3 eV PL, whereas the deposited material just outside the crater could yield either 2.2–2.3 or 2.0 eV signals in different points, as shown in Fig. 3(b). Furthermore, it was difficult to draw any dependence of PL peak position on a number of laser shots. In contrast, PL signals from the porous samples produced by IR optical breakdown exhibited only 1.95 eV signals, whose intensity was stronger than in the case of the excimer ablation by at least an order of magnitude. In contrast to the excimer ablation case, these PL signals were uniform over the treated surface. It should be noted that the PL signals were independent of the extent of the surface treatment, type of silicon wafer (n- or p-) and doping level, corresponding to resistances varying from 0.01 to 10 Ω cm.

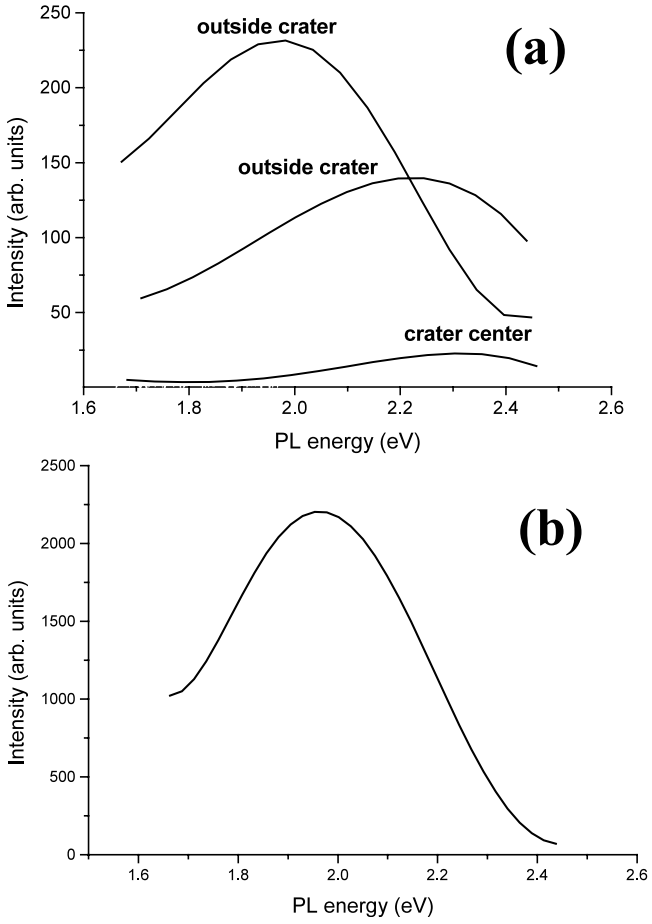


Fig. 3. (a) Typical PL spectra from different regions of the target surface after 500 shots of the excimer laser. (b) Typical PL spectra from the Si-based layer fabricated by the breakdown processing of a silicon wafer by 500 laser shots.

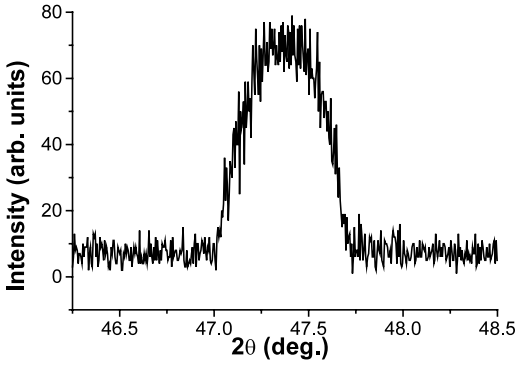


Fig. 2. Highly resolved XRD spectrum near a crystalline Si peak, which appeared as a result of the breakdown processing. To enhance XRD signal, a processed area of $5 \times 5$ mm$^2$ was produced on a silicon wafer by shifting the laser beam over the target.

## 4. Discussion

The difference of properties of layers produced by UV and IR laser irradiation of silicon is related to different conditions and parameters of plasma-assisted processes. Since UV radiation is well absorbed by the silicon target, it leads to an efficient ablation of the target material and to a plasma production. However, the plasma itself does not absorb strongly the UV radiation power and remains almost transparent to the incoming radiation. Therefore, the ablation of material remains efficient during the whole laser pulse, while the ablated material then suffers fast cooling due to collisions with dense air elements, yielding to its deposition on the surrounding target surface. The formation of spikes due to the multi-pulse irradiation is probably related to the difference in absorption efficiency in different regions of the forming relief [16].

On the other hand, the interaction of the IR laser pulse with matter is characterized by a strong photon absorption by the plasma itself. The target generates initial electrons and the ionization develops in a cold gas toward the focusing lens, while the main radiation is absorbed at the forefront of the shock wave through the inverse Bremsstrahlung mechanism [15]. At some moment, the plasma becomes hardly transparent to incoming radiation and gets heated up to the temperatures of about $10^4$ K, while the laser-related ablation of material almost stops. After the laser pulse, the shock wave transforms to a gradually decaying 'fireball', which can live several milliseconds and is characterized by an intense light emission, generation of ultra-strong currents (with magnitudes up to $10^6$ A) [18] and appearance of various electromagnetic phenomena [19–21]. It is proposed that the action of radiation leads to a localized melting and even flash evaporation of the target material. This process probably takes place only in some casual points, which causes the appearance of pores on the target surface. The laser-ablated material and the upper target layer are then heated by the hot breakdown plasma or its currents during milliseconds, leading to additional phase transformations and the initiation of chemical reactions in the plasma. Since the radiation is pulsed, one can assume recrystallization or local vapor redeposition of the material during the off-times. The combined action of laser- and plasma-related processes gives rise to a modification of properties of Si-based compounds formed on the surface and their nanostructuring.

It seems that the mechanism of surface treatment in our experiments is similar in many respects to that of the electric spark processing, which was also used for the fabrication of Si-based nanostructured layers [8–11]. The spark-treated silicon also contained 10–500 nm holes and pores and consisted of silicon nanocrystals embedded in $SiO_2$ matrix (the presence of nanometer-size crystals was confirmed by TEM studies [10]). The modifications were attributed to pulsed ion bombardment of silicon surfaces, which led to a flash evaporation of the target material and its recrystallization during the off-times. Furthermore, the nanostructured layers fabricated by the electric spark processing in pure oxygen also exhibited 1.9 eV signals [8,9,11], though they were relatively weak and fast-degrading [11]. However, the origin of these signals is still not clear. Some properties of 1.9 eV signals such as the degradation behavior [11] enabled to attribute them to a radiative relaxation of excited oxygen atoms originating from the dissociation of ozone molecules [22], whereas other properties [9] give evidence for the mechanism of a radiative recombination between quantum confined states in the nanoscale particles [1]. To identify clearly the PL mechanism, a more detailed study of mechanical, structural and PL properties is now in progress.

## 5. Conclusion

We compared structural and PL properties of nanostructured layers produced by the direct material ablation in atmospheric air and by the air optical breakdown processing. The UV laser ablation led to a formation of microscale spikes under the irradiation spot and to a deposition of material around it. The treated material contained silicon nanocrystals and exhibited weak and non-uniform PL with peaks ranging from 2.0 to 2.3 eV. In contrast, air optical breakdown processing using IR laser radiation led to a formation of a highly porous nanostructured layer under the irradiation spot. The layer exhibited much more intense 1.95 eV PL signals, which were uniform over its surface. The difference of properties of layers prepared by the two methods was attributed to a difference of plasma properties due to different radiation absorption mechanisms.

## Acknowledgements

The authors are grateful to R. Leonelli for assistance during PL studies and to J.-P. Levesque for a technical assistance. The work was supported by Natural Sciences and Engineering Research Council of Canada (NSERC).

## References

[1] L.T. Canham, Appl. Phys. Lett. 57 (1990) 1046.
[2] H. Takagi, H. Ogawa, Y. Yamazaki, A. Ishizaki, T. Nakagiri, Appl. Phys. Lett. 56 (1990) 2379.
[3] Y. Kanemitsu, T. Ogawa, K. Shiraishi, K. Takeda, Phys Rev. B 48 (1993) 4883.

[4] I.A. Movtchan, R.W. Dreyfus, W. Marine, M. Sentis, M. Autric, G. Le Lay, N. Merk, Thin Solid Films 255 (1995) 286.
[5] Y. Yamada, T. Orii, I. Umezu, S. Takeyama, T. Yoshida, Jpn. J. Appl. Phys. 1 (Pt. 35) (1996) 1361.
[6] A.V. Kabashin, M. Meunier, R. Leonelli, J. Vacuum Sci. Technol. B 19 (2001) 2217.
[7] A.V. Kabashin, J.-P. Sylvestre, S. Patskovsky, M. Meunier, J. Appl. Phys. 91 (2002) 3248.
[8] R.E. Hummel, S.-S. Chang, Appl. Phys. Lett. 61 (1992) 1965.
[9] E.F. Steigmeier, H. Auderset, B. Delley, R. Morf, J. Luminescence 57 (1993) 9.
[10] R.E. Hummel, A. Morrone, M. Ludwig, S.-S. Chang, Appl. Phys. Lett. 63 (1993) 2771.
[11] M.H. Ludwig, A. Augustin, R.E. Hummel, Semicond. Sci. Technol. 12 (1997) 981.
[12] K.M.A. El-Kader, J. Oswald, J. Koka, V. Chab, Appl. Phys. Lett. 64 (1994) 2555.
[13] Z. Wang, J. Li, X. Huang, L. Wang, J. Xu, K. Chen, Solid State Commun. 117 (2001) 383.
[14] A.V. Kabashin, M. Meunier, Appl. Surf. Sci. 186 (2002) 578.
[15] Yu.P. Raizer, Laser-Induced Discharge Phenomena, Consultants Bureau, New York, 1977.
[16] D.J. Krajnovich, J.E. Vazquez, J. Appl. Phys. 73 (1993) 3001.
[17] B.D. Cullity, Elements of X-ray Diffraction, Addison-Wesley, Reading, MA, 1978.
[18] M.G. Drouet, H. Pepin, Appl. Phys. Lett. 28 (1976) 426.
[19] V.V. Korobkin, R.V. Serov, JETP Lett. 4 (1966) 70.
[20] A.V. Kabashin, P.I. Nikitin, Quant. Electron. 27 (1997) 536.
[21] A.V. Kabashin, P.I. Nikitin, W. Marine, M. Sentis, Appl. Phys. Lett. 73 (1998) 25.
[22] K. Awazu, H. Kawazoe, J. Appl. Phys. 68 (1990) 3584.